


## RESEARCH ARTICLE OPEN ACCESS

# Cell Seeding Strategy Influences Metabolism and Differentiation Potency of Human Induced Pluripotent Stem Cells Into Pancreatic Progenitors

Hui Huang<sup>1</sup> | Kaiming Ye<sup>1,2</sup> | Sha Jin<sup>1,2</sup> 

<sup>1</sup>Department of Biomedical Engineering Thomas J. Watson College of Engineering and Applied Science Binghamton University, State University of New York (SUNY), Binghamton, New York, USA | <sup>2</sup>Center of Biomanufacturing for Regenerative Medicine, Binghamton University, State University of New York (SUNY), Binghamton, New York, USA

**Correspondence:** Sha Jin ([sjin@binghamton.edu](mailto:sjin@binghamton.edu))

**Received:** 10 February 2025 | **Revised:** 18 March 2025 | **Accepted:** 9 April 2025

**Funding:** This work was partially supported by National Institutes of Health EB027391-01; National Science Foundation CBET1919830 and CBET1928855.

**Keywords:** cell seeding | differentiation | human induced pluripotent stem cells | metabolism | oxygen consumption | pancreatic progenitors

## ABSTRACT

Human induced pluripotent stem cells (iPSCs) are an invaluable endless cell source for generating various therapeutic cells and tissues. However, their differentiation into specific cell lineages, such as definitive endoderm (DE) and pancreatic progenitor (PP), often suffers from poor reproducibility, due partially to their pluripotency. In this work, we investigated the impact of iPSC confluency during cell self-renewal and seeding density on cell metabolic activity, glycolysis to oxidative phosphorylation shift, and differentiation potential toward DE and PP lineages. Our findings demonstrated that cell seeding strategy influences cellular metabolic activity and the robustness of iPSC differentiation. iPSCs maintained at higher seeding density exhibited lower initial oxygen consumption rate (OCR) and metabolic activity. There is an optimal seeding density to ensure sufficient oxygen consumption during differentiation and to yield high expression of SOX17 in the DE lineage and high PDX1/NKX6.1 dual-positive cells in PPs. Interestingly, we found that cell confluency at the time of harvest has less impact on the efficacy of pancreatic lineage formation or metabolic activity. This study sheds light on the interplay between metabolic activity and iPSC lineage specification, offering new insights into the robustness of iPSC self-renewal and differentiation for creating human tissues.

## 1 | Introduction

The advent of induced pluripotent stem cells (iPSCs) provides an unlimited source for generating various types of cells and tissues for diverse applications [1–4]. Nevertheless, iPSC differentiation exhibited poor reproducibility, due partially to their pluripotent nature. This has become a persistent issue, especially in directing iPSCs into definitive endoderm (DE), pancreatic progenitors (PPs), and subsequently, functional endocrine cells. The DE lineage is the first and crucial step for PP specification, with its yield varying significantly. Three protocols were compared and demonstrated distinct differentiation efficiency, characterized by

PDX1/NKX6.1 co-expressing cell population [5]. Research groups, including us, have explored varied strategies to increase the yield of DE cells, PPs, and endocrine  $\beta$  cells. These approaches included but not limited to the optimization of growth factors and signaling molecules [6–11], cultivation from 2D to 3D environment [12, 13], and using green fluorescent protein (GFP) reporter to purify GFP-expressing PPs before further differentiation into  $\beta$  cells [14].

It is well-documented that the fate of iPSCs is modulated by a multitude of physiochemical factors, such as dissolved oxygen, biomechanical stimuli, and signaling molecules. These factors constitute as a cellular microenvironment to synergistically

This is an open access article under the terms of the [Creative Commons Attribution-NonCommercial-NoDerivs](https://creativecommons.org/licenses/by-nc-nd/4.0/) License, which permits use and distribution in any medium, provided the original work is properly cited, the use is non-commercial and no modifications or adaptations are made.

© 2025 The Author(s). *Biotechnology Journal* published by Wiley-VCH GmbH.

regulate embryonic stem cell (ESC) differentiation [15]. In the stem cell culture microenvironment, cell-cell contact uniquely affects differentiation potency, which is considered as epigenetic memory established during the culture [16, 17], and the former could be modulated by altering cell seeding density and colony size [18]. Another important parameter in maintaining stem cell pluripotency for differentiation is the oxygen level. While pluripotency of stem cells can be readily maintained under both hypoxic and normoxic conditions, hypoxia reduces the degree of spontaneous stem cell differentiation during cell maintenance [19]. By contrast, normoxic or hyperoxic conditions favor iPSC differentiation to DE and pancreatic lineages [13, 20, 21], which promote the endocrine progenitors' development [13, 22]. Meanwhile, cell metabolic activity is directly associated with developmental trajectory, governing the differentiation progression [23]. Glycolysis and oxidative phosphorylation pathways are two dominant metabolic pathways through which cells produce energy. A substantial switch from glycolysis to oxidative phosphorylation signifies iPSC differentiation [24]. This phenomenon has been mechanistically evidenced by the involvement of a mitochondrial protein, uncoupling protein 2 (UCP2) to control the shift [25]. Therefore, the switch in metabolic pathways is a signature feature in cell metabolism between stem cells and differentiated cells.

It has been reported that stem cell density plays an important role in brain microvascular endothelial cell differentiation [26] and there is an optimal seeding density for osteoblasts specification from human umbilical cord mesenchymal stem cells [27]. However, the effects of iPSC expansion and seeding on DE and PP differentiation remain largely unknown. In this study, we aimed to elucidate these effects to enhance the robustness of iPSC differentiation. We examined the impact of iPSC expansion on oxygen metabolic activity, the shift in metabolic pathways, and their differentiation into pancreatic lineages.

## 2 | Materials and Methods

### 2.1 | iPSC Culture and Differentiation

Human iPSC line IMR90 was obtained from WiCell Research Institute. Cells were maintained on growth factor reduced Matrigel (Corning Life Science) coated dishes in mTeSR1 medium (StemCell Technologies), as detailed in our previous study [28]. Cells were passaged every 2 to 3 days using Dispase (StemCell Technologies). They were passaged onto Matrigel-coated dishes with high or low densities to achieve a final 70%–80% confluency for a high confluent culture and 40%–50% confluency for a low confluent condition at the time of harvest. To initiate differentiation, cells were harvested for single cell seeding using Accutase (StemCell Technologies) and seeded on a Matrigel-coated cell culture plate with 0.2, 0.5, and 0.8 million cells/mL seeding densities, respectively. The DE and PP differentiation were carried out using a protocol developed in our previous studies [28, 29].

### 2.2 | Detection of the Distribution of Dissolved Oxygen at Cell Bed

An optical oxygen sensor foil system was used to measure the dissolved oxygen concentration at the cell bed. The oxygen

sensor foil (SF-RPSu4) (PreSens, Regensburg, Germany) contains a green reference dye and a red indicator dye. As the detect unit (DU01) (VisiSens, PreSens, Regensburg, Germany) gives out a blue excitation light, oxygen reacts with the indicator dye, leading to luminescence quenching. The sensor foil was calibrated for 100% and 0% saturated air (s.a.) calibration point, that is, 20.9% in the air and 0% in nitrogen gas. Therefore, 100% s.a. readout by the sensor indicates 20.9% of oxygen in the air. Briefly, a piece of sensor foil was placed into a glass bottle. The 100% s.a. point was recorded when the glass bottle was opened in the atmospheric air, whereas the 0% s.a. point was recorded when the glass bottle was filled with nitrogen. The sensor foil was adjusted to fit the shape of a well of a 48-well cell culture plate to measure the oxygen concentration. A total of 70% ethanol was used to sterilize the sensor before use. A silicone gel was used to prevent the floating and moving of the foil. The foil-containing plate was coated with Matrigel (80 µg/mL) before seeding. iPSCs harvested from a high or low confluent culture were seeded on the surface of the sensor foil post 1 h of Matrigel-coating and cultured in mTeSR1 in a CO<sub>2</sub> incubator at 37°C. The initial oxygen consumption rate (OCR) was defined as the change in oxygen concentration over initial 2 or 3 h per the number of cells. Immediately before detecting the dissolved oxygen concentration, the culture medium was replaced with prewarmed 2% (w/v) bovine serum albumin (BSA) in a Dulbecco's phosphate buffered saline (DPBS) (HyClone). The cell culture plate was then sealed with a tape and placed into a glove box filled with nitrogen. All the measurements and recordings were conducted in a dark environment. The dissolved oxygen was recorded every hour over a period of five hours and analyzed using the Data Viewer software (PreSens). To estimate initial OCR, the dissolved oxygen concentration was calculated using Henry's Law  $C = k_H \times P_{O_2}$ , where  $C$  is the dissolved oxygen concentration,  $k_H$  is the Henry's Law constant, and  $P_{O_2}$  is the partial pressure of oxygen. The results were normalized to per 10,000 cells per min.

### 2.3 | Assessment of Mitochondrial Metabolic Activity

A cell proliferation reagent WST-1 kit (Cayman Chemicals) was used to quantify cellular metabolic activity of mitochondria according to the manufacturer's instructions. It is also an indication of cell viability, as it is directly proportional to the viable cell number. A BioTek Cytation 5 Cell Imaging Multimode Reader was used to detect optical density (OD) at 450 nm.

### 2.4 | Assessment of Glycolysis and Oxidative Phosphorylation Pathways

The metabolic pathways were quantified by an ATP assay kit (Dojindo Laboratories) and a lactate meter system (The EDGE) according to the manufacturers' instructions. The oligomycin (OG) and the 2-deoxy-D-glucose (2-DG) (Sigma) were used to inhibit the oxidative phosphorylation and glycolysis, respectively. The iPSCs maintained at high or low confluent conditions were seeded in a white 96-well plate with varied initial seeding densities. Cells were treated with 1.25 µmol/L OG or 22.5 mmol/L 2-DG for 5 h prior to the measurement. The luminescence signal was recorded and analyzed by the BioTek Cytation 5 Cell Imaging Multimode Reader.

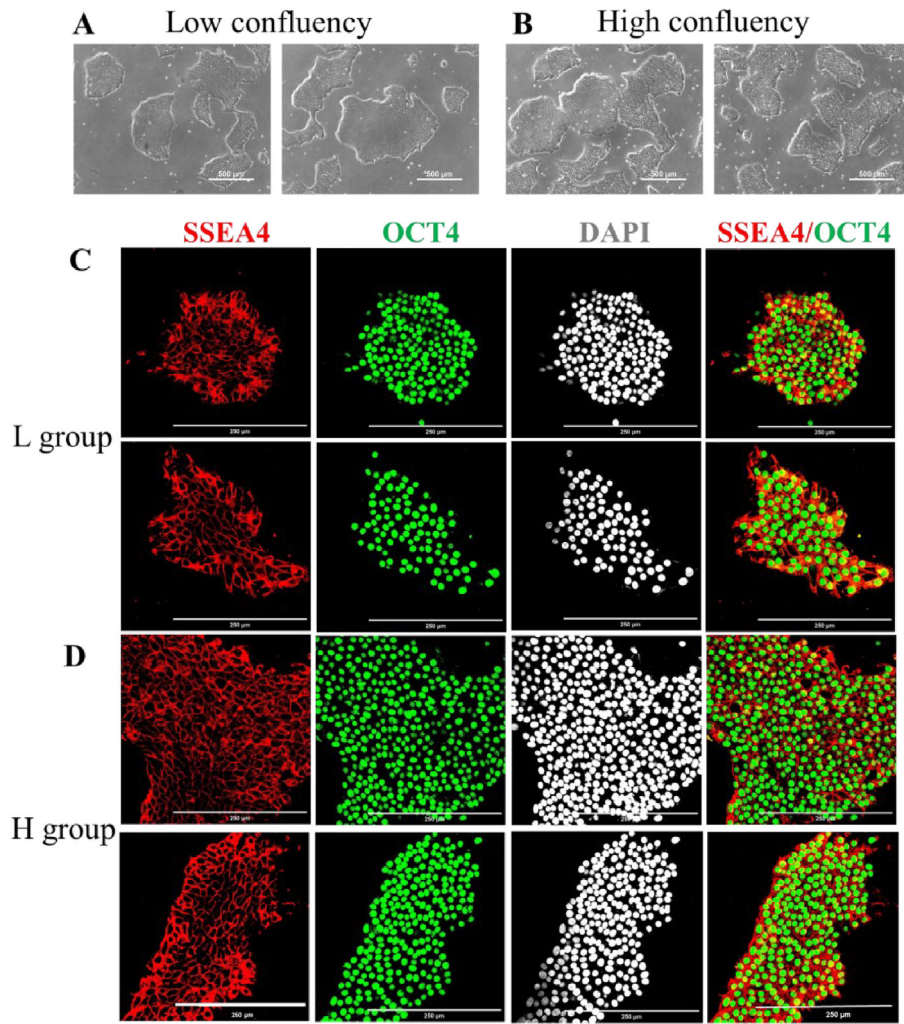


**FIGURE 1** | The expression of pluripotent markers in iPSCs maintained under low (L) or high (H) confluency. (A and B) Phase-contrast micrographs of iPSCs under low or high confluency. (C and D) Fluorescence images of SSEA4 (red) and OCT4 (green) expressions in iPSCs cultured under low or high confluency. Cells were counterstained with diaminophenylindole (DAPI) (grey). Scale bars: 250 μm.

## 2.5 | Flow Cytometry

Flow cytometry was carried out, as described in our previous study [11]. Briefly, differentiated cells were rinsed twice with DPBS and then incubated with TrypLE Express enzyme (Gibco) at 37°C for 6–8 min. The enzyme reaction was neutralized with DMEM/F12 medium containing 10% of fetal bovine serum. The dissociated cells were collected and washed twice with DPBS. For intracellular antibody staining, single cells were fixed in Foxp3 fixation/permeabilization working solution in the dark at room temperature for 30 min. Fixed cells were washed three times in a permeabilization buffer, followed by blocking with 5% goat serum containing permeabilization buffer at 4°C for 30 min. After blocking, the cells were incubated with conjugated, primary, or isotype control antibodies at 4°C for 1 h, followed by wash with the permeabilization buffer. Secondary antibodies prepared in the permeabilization buffer were added to the cells and incubated at 4°C for 1 h. The cells were then washed three times with the permeabilization buffer and stored in 2% (w/v) BSA-containing DPBS buffer for data acquisition using a ZE5 Cell Analyzer (Bio-Rad). The acquired data were analyzed by FlowJo software. Detailed antibody information used were listed in Table S1.

## 2.6 | Immunofluorescence Microscopy

The immunostaining and confocal imaging were performed, as described previously [6]. The iPSCs were seeded into 8-well glass bottom chambers and cultured in mTeSR1. Immunofluorescence microscopy was performed by staining cells with primary antibodies at 4°C overnight, followed by wash three times with PBS at room temperature to remove excess antibodies. Secondary antibodies were then applied at room temperature for 1 h, followed by wash three times with PBS. The samples were stained for nucleus with Vectashield Mounting Medium containing DAPI (Fisher Scientific). The antibodies used in this study were listed in Table S1.

## 2.7 | Statistical Analysis

The experimental results were presented as the mean  $\pm$  standard deviation (SD) for a minimum of three independent experiments. Statistical analyses comparing different groups were performed using a two-tailed unpaired Student's *t*-test.  $p < 0.05$  was considered statistically significant.



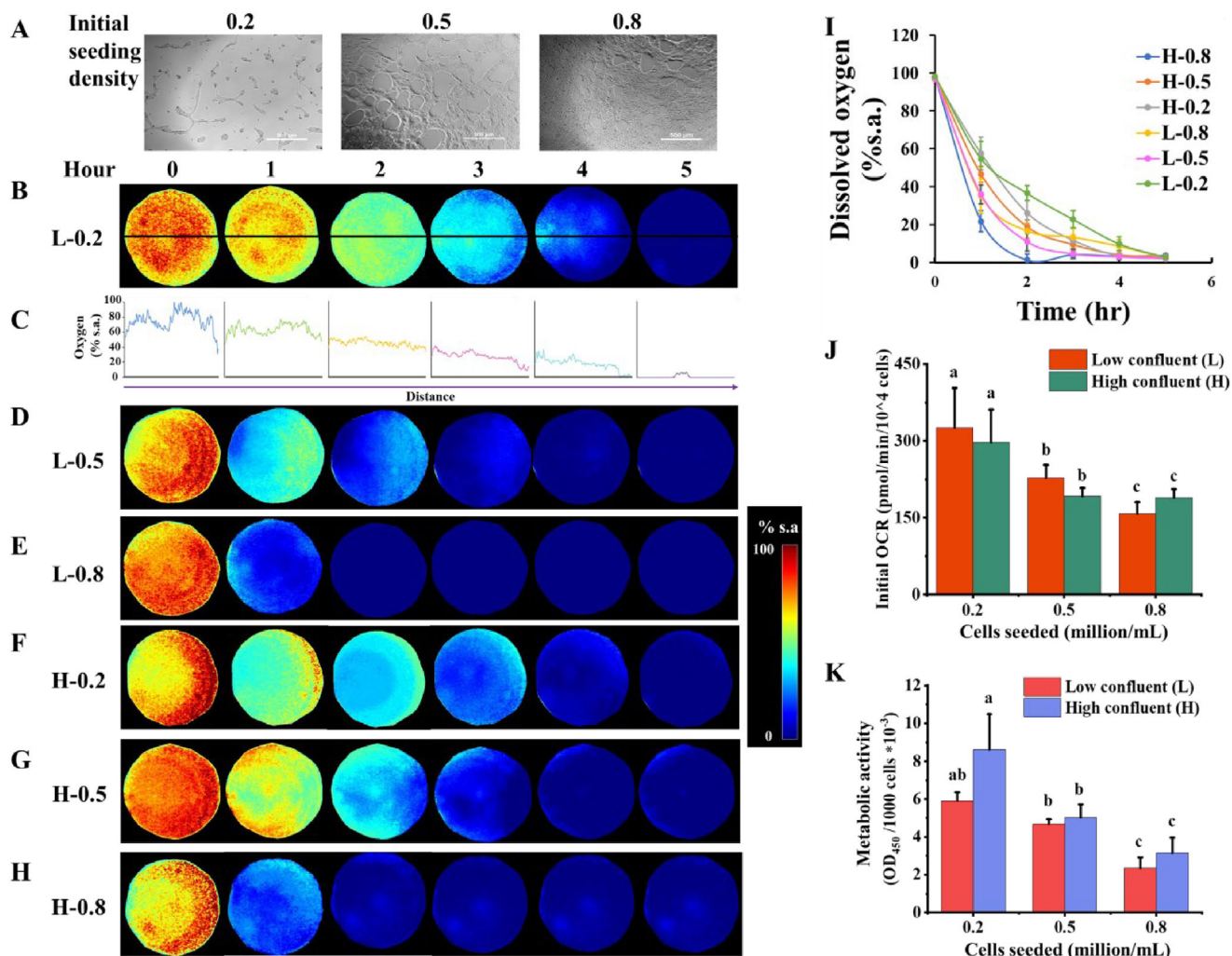


**FIGURE 2** | Mapping initial OCR at the cell bed and iPSCs' metabolic activity under varied seeding strategies. (A) The cell confluent levels after overnight culture under seeding densities of 0.2, 0.5, and  $0.8 \times 10^6$  cells/mL. (B–H) Distribution of dissolved oxygen levels under varied seeding densities. (B–E) L-0.2, L-0.5, L-0.8: cells collected from a low confluent group and seeded at 0.2, 0.5, and  $0.8 \times 10^6$  cells/mL, respectively. (C) Dissolved oxygen levels along a center line of the cell bed indicated by the line in (B). (F–H) H-0.2, H-0.5, and H-0.8: cells harvested from a high confluent group and seeded at 0.2, 0.5, and  $0.8 \times 10^6$  cells/mL, respectively. (I) The change of dissolved oxygen level under varied conditions. (J) Initial OCR normalized to  $10^4$  cells. (K) Cell mitochondrial activity normalized to 1000 cells. Results were shown as mean  $\pm$  SD from three independent experiments.  $n = 3$  for each group. Different letters above each bar indicate significant difference.

### 3 | Results

#### 3.1 | The Effect of Confluence and Seeding Density on iPSC Metabolic Activity and Initial OCR

Seeding density associates with cell–cell contact that can influence cell lineage specification and differentiation. However, its actual impact on iPSC pancreatic differentiation remains largely elusive. Thus, we carried out a series of experiments to ascertain how DE differentiation, one of the most crucial steps toward pancreatic endocrine cells from iPSCs, is affected by the seeding strategy. First, we determined whether the iPSCs exhibit any spontaneous differentiation when they are maintained under low (L) (40%–50%) or high (H) (70%–80%) confluency. As illustrated in Figure 1, iPSCs in both L and H groups remained undifferentiated and expressed pluripotent stem cell markers SSEA4 and OCT4. The high-level expression of these pluripotent stem cell

markers alluded a well-maintained pluripotent state under varied confluent conditions.

Next, we assessed the impact of seeding strategy on iPSC metabolic activity, including an initial OCR at the cell bed, as described in Section 2. Both low and high confluent populations were harvested and seeded at densities of 0.2, 0.5, and 0.8 million cells per milliliter. After overnight culture, the cells reached approximately 20%–30%, 50%–60%, and 80%–90% confluences, respectively (Figure 2A). These varied confluent levels provide a controllable environment to examine how different seeding densities influence cell metabolism and subsequent differentiation. We monitored the cellular initial OCR at cell bed real-time using a novel oxygen mapping sensor. We observed a rapid (within a few hours) depletion of oxygen in both L and H groups (Figure 2B–H). However, oxygen depleted faster in the groups with higher seeding densities (Figure 2D,E,H). As

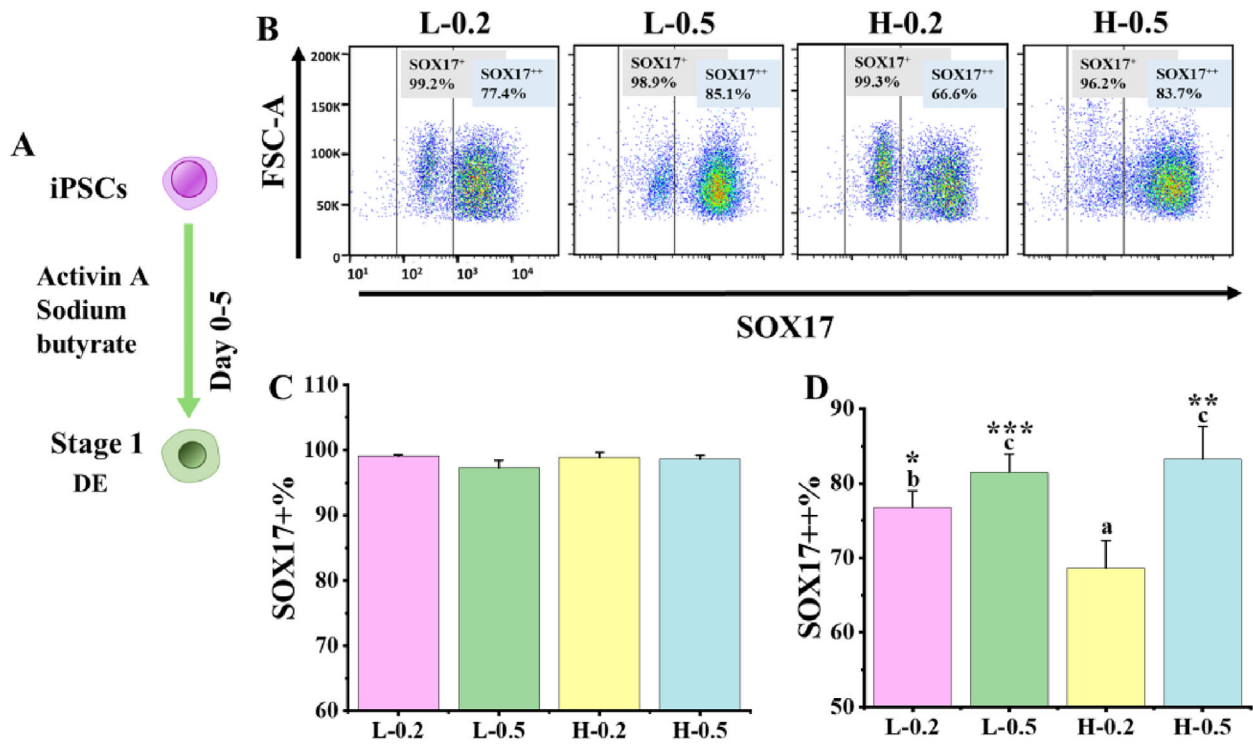


**FIGURE 3 |** The effect of different seeding strategies on DE differentiation. (A) A schematic diagram of DE differentiation from iPSCs. (B) Flow cytometric analysis of SOX17 expression on day 5. A large box shows the percentage of SOX17<sup>+</sup> cell subpopulation and a small box indicates a cell subpopulation with higher SOX17 expression (SOX17<sup>++</sup>). (C and D) Percentages of SOX17<sup>+</sup> and SOX17<sup>++</sup> cells in DE ( $n = 3$ ). Results were from three independent experiments and shown as mean  $\pm$  SD. \* $p < 0.05$ , \*\* $p < 0.01$ , and \*\*\* $p < 0.001$ . Different letters above each bar indicate significant difference.

an example of measurement, Figure 2C displays the alteration of the dissolved oxygen level along the central axis of the cell bed in the L-0.2 group that is depicted by the line in Figure 2B.

Following these measurements, we determined a time course of average oxygen depletion under each condition (Figure 2I). At a seeding density of  $0.8 \times 10^6$  cells/mL in the high confluence group (H-0.8), the oxygen diminished rapidly from 98% s.a. to 21% s.a. within 1 h. In contrast, the dissolved oxygen in the cell bed seeded at the same density ( $0.8 \times 10^6$  cells/mL) but from a low confluence group (L-0.8) reduced to 35% s.a. within 1 h (Figure 2I). iPSCs seeded at  $0.2 \times 10^6$  cells/mL in both L- and H- groups exhibited a comparatively slower decline in the dissolved oxygen level. There was  $\sim 20\%$  s.a. available over 2.4 h in H-0.2 and 3.3 h in L-0.2 group, respectively. Interestingly, iPSCs seeded at low density tended to have a higher initial OCR (Figure 2J). Cells collected from low confluence group (L-0.2) and seeded at a density of  $0.2 \times 10^6$  cells/mL showed an initial OCR of  $326 \pm 77.5$  pmol/min/10,000 cells. In contrast, cells from high confluence group (H-0.2), seeded at the same density, exhibited an initial OCR of  $297 \pm 64.1$  pmol/min/10,000 cells, suggesting that the cells collected under low confluency are more metabolically active when seeded at a low density. The initial OCR was  $189.3 \pm 16.5$  pmol/min/10,000 cells for cells collected under high confluency and seeded at  $0.8 \times 10^6$  cells/mL (H-0.8), where it dropped to  $157.8 \pm 22.6$  pmol/min/10,000 cells for cells collected under low confluency and seeded at the same density (L-0.8) (Figure 2J). Nevertheless, the overall metabolic activities reduced with an increase in the seeding density. Examining the

mitochondrial activities of iPSCs seeded under different strategies confirmed this observation (Figure 2K).

### 3.2 | The Effect of iPSC Seeding Strategy on Definitive Endoderm Differentiation

To investigate whether iPSC seeding strategy influences iPSC differentiation to DE, we collected iPSCs under different confluency and seeded them at densities of 0.2, 0.5, and  $0.8 \times 10^6$  cells/mL, respectively, followed by inducing differentiation to DE, as shown in Figure 3A. We observed massive cell death when seeding at a high density ( $0.8 \times 10^6$  cells/mL) from both L and H groups, implying the cell death and failure in the DE differentiation due to insufficient oxygen supply with such seeding densities. Analyzing DE marker, SOX17 expression revealed 99.1% SOX17<sup>+</sup> cells in the L-0.2 group and 97.3% in the L-0.5 group. The percentage of SOX17<sup>+</sup> cells formed from the H-0.2 and H-0.5 groups were almost the same. They were 98.9% in the H-0.2 group and 98.6% in the H-0.5 group (Figure 3B,C). Interestingly, we observed two subpopulations of DE cells, that is, low (+) and high (++) SOX17 expressing cells differentiated from iPSCs under different seeding strategies. There were  $81.5 \pm 1.2\%$  SOX17<sup>++</sup> in the L-0.5 group and  $83.2 \pm 4.4\%$  SOX17<sup>++</sup> cells in the H-0.5 group, significantly higher than that in the L-0.2 ( $76.8 \pm 2.2\%$ ) and H-0.2 ( $68.6 \pm 3.7\%$ ) groups. The different level of SOX17-expressing cells in iPSC-DE suggests their different capacities for subsequent organ development. Taken together, our experimental results indicated that the cell confluent level at the time of harvest does not exert significant impact on DE differentiation. In contrast, the seeding density is

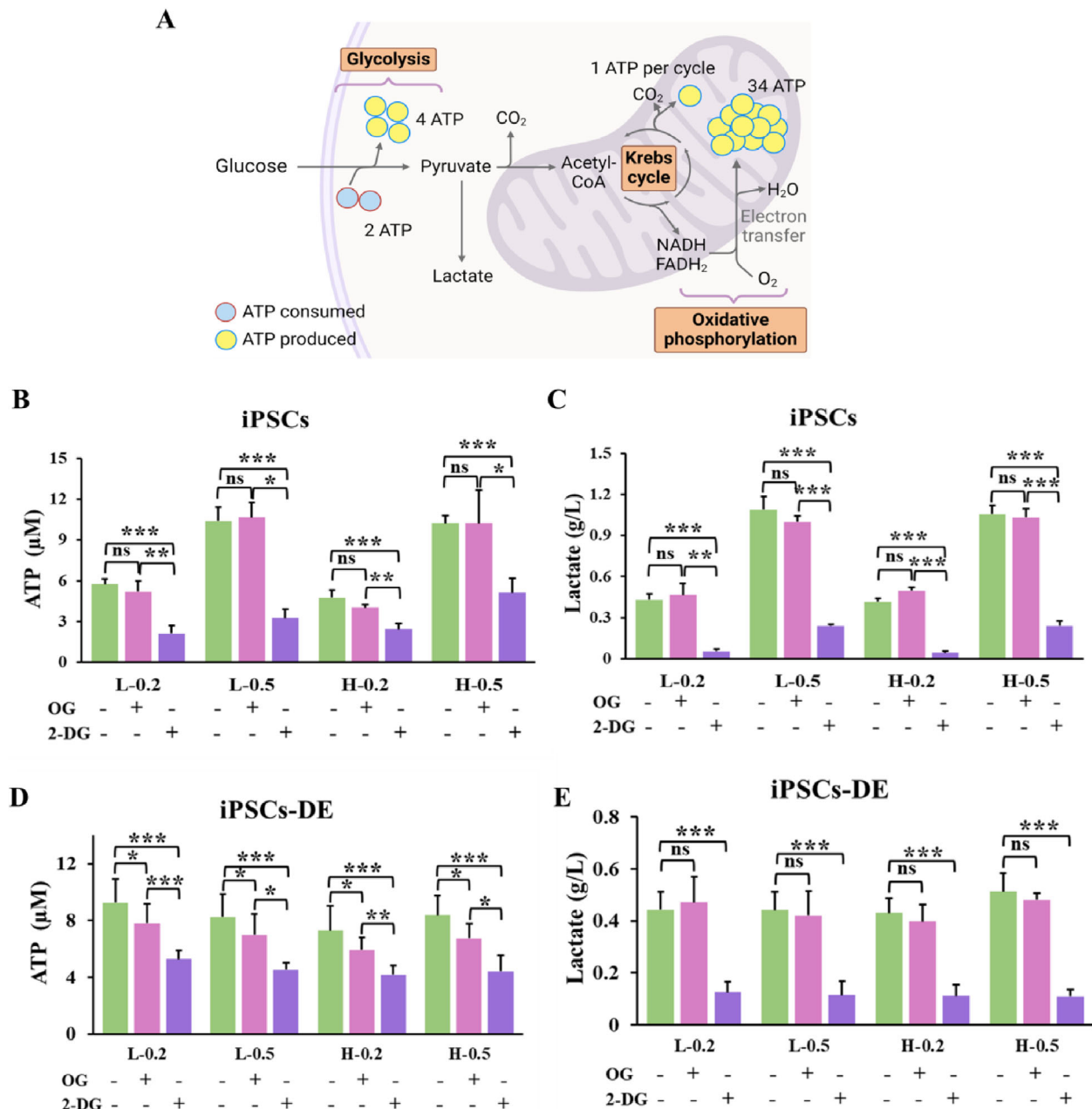


**FIGURE 4** | The effect of iPSC seeding strategy on energy metabolic pathways before and after DE formation. (A) A schematic diagram of aerobic cell respiration pathways. (B–E) ATP and lactate production from iPSCs under varied seeding densities before DE differentiation (B and C). (D and E) ATP and lactate production at the end of DE formation under varied seeding densities. 2-DG inhibits glycolysis, whereas OG suppresses the ATP synthesis in oxidative phosphorylation. Results were shown as mean  $\pm$  SD from three independent experiments ( $n = 3$  for each group). \* $p < 0.05$ , \*\* $p < 0.01$ , and \*\*\* $p < 0.001$ . ns: not significant.

crucial for DE differentiation. A high seeding density causes cell death during DE differentiation presumably due to insufficient oxygen supply. Therefore, L- and H-0.8 conditions were not further tested,

### 3.3 | Alternation of Energy Production Before and After DE Formation Under Varied iPSC Seeding Strategies

Next, we determined whether iPSC seeding strategy influences energy production during iPSC maintenance or DE differentia-

tion. In cellular respiration, glucose is initially broken down into pyruvate through glycolysis. Two ATP molecules are consumed in breaking down of one glucose molecule, and four ATP molecules are generated, resulting in a net production of two ATP molecules from the breakdown of one glucose molecule. Lactate is a typical by-product of the glycolysis pathway (Figure 4A). Pyruvate generated in glycolysis is metabolized through either aerobic glycolysis to generate lactate or enters the Krebs cycle and subsequent pathway of oxidative phosphorylation inside the mitochondrion [30]. Through the Krebs cycle, pyruvate is consumed to provide NADH for oxidative phosphorylation for ATP production. Therefore, we monitored ATP and lactate production in order



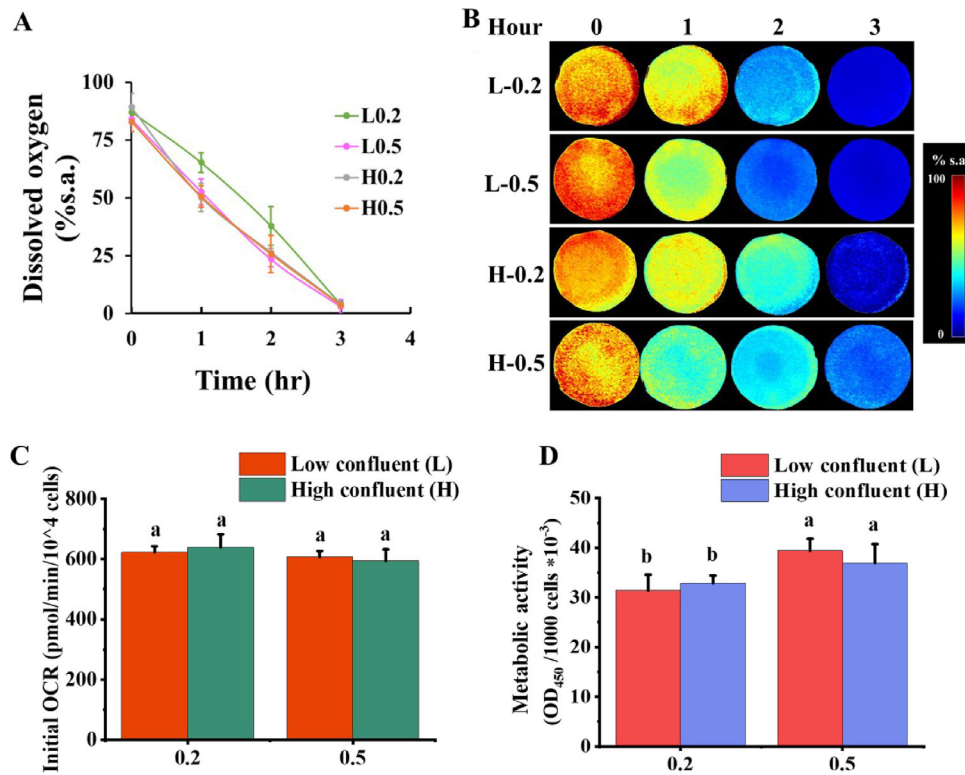


**FIGURE 5** | Comparison of the oxygen consumption and metabolic activity of iPSC-derived definitive endoderm under varied seeding strategies. (A) The change of dissolved oxygen levels in DE under varied seeding strategies. (B) Oxygen mapping in DE under varied conditions. (C) Initial OCR in DE calculated per 10,000 cells. (D) Cell mitochondril activity normalized to 1000 cells. Results were from three independent experiments and shown as mean  $\pm$  SD. ( $n = 3$  for each group). Different letters above each bar indicate significant differences.

to ascertain a potential metabolic pathway shift before and after DE differentiation from iPSCs seeded under varied conditions. Particularly, we used 2-DG and OG to inhibit glycolysis and oxidative phosphorylation pathways, respectively. We discovered that the inhibition of the oxidative phosphorylation pathway did not affect ATP or lactate production (Figure 4B,C). Noticeably, blocking glycolysis pathway by 2-DG resulted in a significant decrease in ATP and lactate productions. Majority of the lactate production was suppressed in 2-DG treated iPSCs (Figure 4C). These results revealed that iPSCs utilize glycolytic pathway for metabolism, which is consistent with previous studies [31, 32]. In addition, we observed approximately 2-fold increase in ATP production from iPSCs cultured at  $0.5 \times 10^6$  cells/mL seeding than that at  $0.2 \times 10^6$  cells/mL seeding (Figure 4B,C). The phenomenon is due to the fact that the L-0.5 and H-0.5 groups have approximately twice the cell amount compared to the L-0.2 and H-0.2 groups. With an increased cell number, there is a corresponding elevation in glucose consumption and concurrent ATP and lactate production. These results suggested that energy metabolic pathway is not affected by cell sending density.

Furthermore, we discovered that ATP production in the DE cells can be significantly suppressed by blocking oxidative phosphorylation pathway with OG and/or the glycolysis pathway with 2-DG (Figure 4D). The glycolysis blockage was more profound in suppressing ATP production. Meanwhile, there was  $\sim 72\%$  of reduction in lactate production if the glycolysis was suppressed in the DE cells (Figure 4E). These experimental results uncovered that the DE cells rely on both the glycolysis and oxidative

phosphorylation for energy production. Thus, we speculated that a metabolic pathway shift occurred before and after DE differentiation. iPSCs primarily utilize the glycolytic pathway to generate energy before DE differentiation, whereas they switch to using both glycolytic and oxidative phosphorylation pathways to generate energy upon iPSC differentiation.

### 3.4 | The Effect of iPSC Seeding Strategy on iPSC-DE's Metabolic Activity

In the next experiment, we examined the influence of cell confluency and seeding density on the metabolic activity of DE cells. To perform these tests, we sealed the plate after the formation of DE cells from iPSCs under different seeding strategies to ensure that no oxygen could diffuse into the plate. We observed that the dissolved oxygen level decreased sharply to almost zero within 3 h in each group tested (Figure 5A,B). We observed that the initial OCR levels under the four conditions were comparable. There were  $623.3 \pm 19.7$  pmol/min/10,000 cells in the L-0.2 group,  $607.5 \pm 19.6$  pmol/min/10,000 cells in the L-0.5 group,  $639 \pm 43.1$  pmol/min/10,000 cells in the H-0.2 group, and  $594.5 \pm 37.7$  pmol/min/10,000 cells in the H-0.5 group (Figure 5C). Remarkably, the initial OCR in DE cells was more than 3-fold higher than that in iPSCs before differentiation (Figure 5C,B), indicating the importance of the oxygen supply for iPSC DE differentiation. The results also suggested that the cellular oxygen consumption remains stable under appropriate seeding density. These observations are in consistence with previous findings that

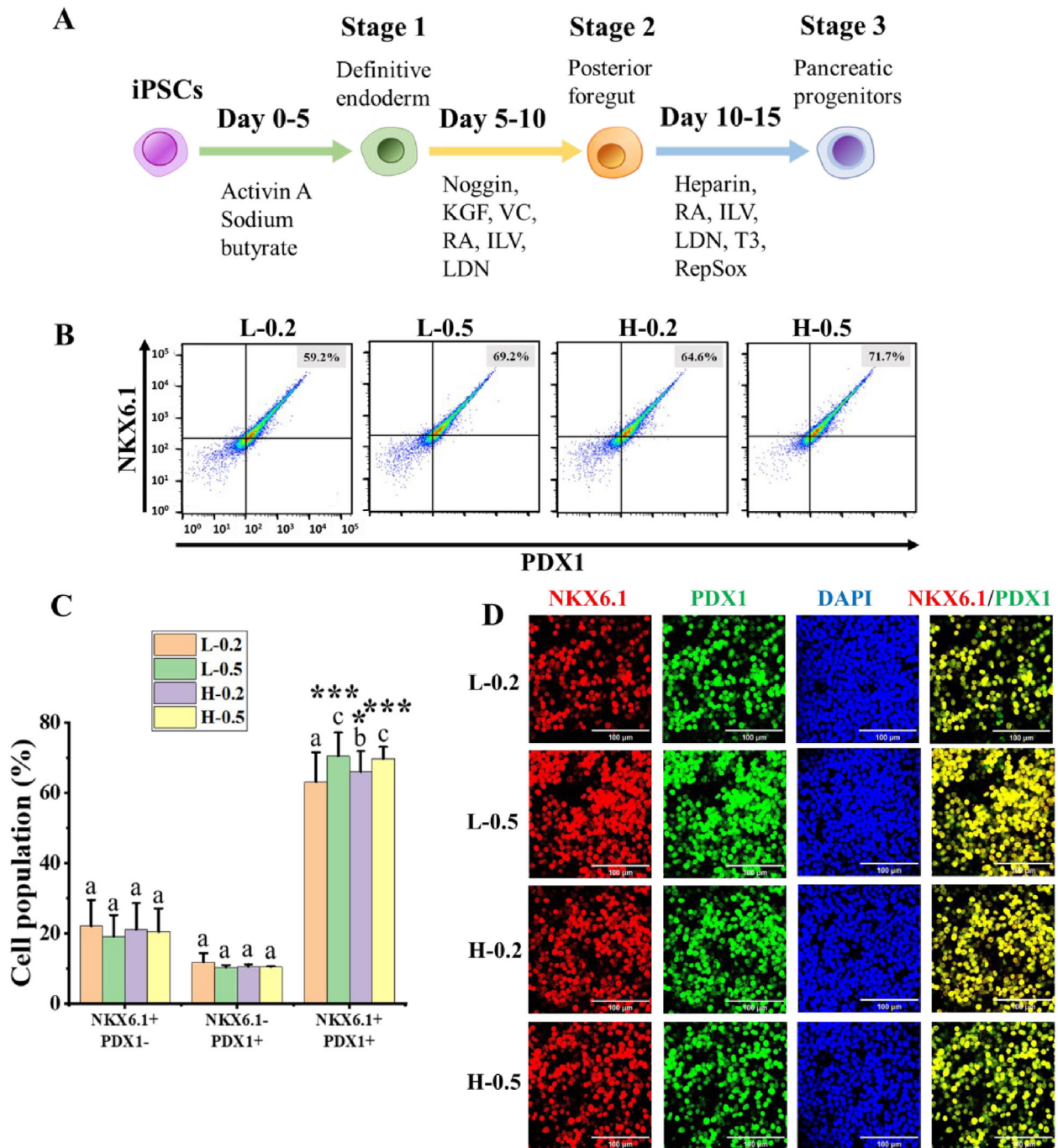


**FIGURE 6** | Differentiation of pancreatic progenitors from iPSCs. (A) A protocol for pancreatic progenitor development from iPSCs. (B) Flow cytometric analysis of PDX1 and NKX6.1 expressing subpopulations in PPs. (C) Average percentage of PDX1<sup>+</sup> NKX6.1<sup>+</sup> cell subpopulation at the end of the differentiation ( $n = 3$ ). (D) Immunofluorescence micrographs of PDX1 (green) and NKX6.1 (red) expressing cells at the end of the PP differentiation. Cells were counterstained with DAPI (blue). Scale bar: 100  $\mu$ m. Results were shown as mean  $\pm$  SD. \* $p < 0.05$  and \*\*\* $p < 0.001$ . Different letters above each bar indicate significant differences.

DE cells are sensitive to available oxygen and the generation of DE from stem cells requires a higher oxygen supply [13, 20]. Additionally, we investigated the mitochondrial activity of iPSC-DE and compared it with iPSCs. As shown in Figure 5D, the DE cells formed from a lower seeding density ( $0.2 \times 10^6$  cells/mL) showed a relatively low metabolic rate compared to those formed from a higher seeding density ( $0.5 \times 10^6$  cell/mL). Notably, the mitochondrial activity in DE cells was 4~8-fold high than that in iPSCs (Figures 2 and 5).

### 3.5 | The Effect of iPSC Seeding Strategy on PP Generation

Furthermore, we interrogated efficiency of PP differentiation under varied seeding strategies using a 3-stage stepwise differentiation protocol (Figure 6A). The efficiency was assessed by determining the percentage of PDX1<sup>+</sup> NKX6.1<sup>+</sup> cells formed at the end of PP differentiation, as PDX1 and NKX6.1 co-expressing cells are able to differentiate into mature endocrine cells [33, 34]. The



dual-color flow cytometric analysis revealed that ~71% cells were PDX1<sup>+</sup> NKX6.1<sup>+</sup> cells at a seeding density of  $0.5 \times 10^6$  cells/mL in both L-0.5 and H-0.5 groups. This number was around 61~65% when seeding density was  $0.2 \times 10^6$  cells/mL in both L-0.2 and H-0.2 groups (Figure 6B,C). The results suggested that confluence level does not affect PP differentiation when cells were seeded at  $0.5 \times 10^6$  cells/mL. However, seeding cells collected from a high confluence group at a low density, such as  $0.2 \times 10^6$  cells/mL, elevated the PDX1<sup>+</sup> NKX6.1<sup>+</sup> cell population to 65% (Figure 6C). The results were confirmed by immunofluorescence microscopic imaging, where majority of the PP cells were PDX1<sup>+</sup> NKX6.1<sup>+</sup>. Therefore,  $0.5 \times 10^6$  cells/mL seeding density resulted in a higher differentiation efficacy of iPSCs into PPs.

## 4 | Discussion

In this study, we discovered that iPSCs consumed oxygen at a high initial OCR when they were seeded at a low density regardless a confluent level when cells were harvested for seeding. This observation implies that a high seeding density can cause iPSC death due to the inability for cells to maintain healthy OCR and mitochondrial activity. This might be due to small cell volume formed under a high seeding density that restricts cell spreading. This speculation is supported by previous study reported by Wagner et al. where they discovered that the initial OCR in mammalian cells is proportional to cell volume [35]. Cells with smaller volume tend to adapt to the environment with a slow oxygen supply, as observed in this study, which is supported by a recent study by Folmes et al. [28]. A rapid oxygen consumption and a low metabolic activity associated with a high seeding density may lead to the failure of DE formation from iPSCs. Thus, seeding density is crucial to DE and PP differentiation. Moreover, we noticed that the level of cell confluency does not affect the metabolic activity rate, suggesting the robustness of cell maintenance (Figure 2K). This phenomenon is similar to a cell line that within a defined range, cells seeded at high density demonstrated a rapid onset of metabolic inactivity [36]. Cells' free NADH or respiration when seeded with a low density markedly exceeds those seeded at a high density [36].

Theoretically, one molecule of glucose breakdown can generate two molecules of ATP from the Krebs cycle and 34 molecules of ATP from the oxidative phosphorylation. An increased demand for ATP during iPSC proliferation leads to an increased aerobic glycolysis, yielding more rapid ATP production [37]. The shift from glycolysis to oxidative phosphorylation pathway is an indication of iPSC differentiation. We observed co-utilization of both glycolysis and oxidative phosphorylation pathways by DE cells. Moreover, an increased initial OCR during DE differentiation compared to iPSC proliferation reveals that DE differentiation requires a higher oxygen supply, which is in agreement with previous findings by other research groups and ours [13, 20]. Our seeding strategy ensured that more than 96% of cells express SOX17 in iPSC-DE, and 70% of cells co-express PDX1 and NKX6.1 in PPs. Additionally, the experimental results imply that undifferentiated iPSCs tolerate to the available oxygen in the culture environment, which support previous finding that iPSCs can be maintained under a hypoxic condition [19]. The study revealed that iPSC seeding strategy directly impacts cell metabolic activity

and differentiation efficiency, which in turn affects robust and reproducible iPSC differentiation into pancreatic lineages.

## 5 | Conclusions

We investigated the effects of iPSCs seeding strategies on DE and PP differentiation, oxygen consumption, and energy metabolic pathways. We found the interplays among seeding densities, iPSC mitochondrial activity, and initial OCR. iPSCs largely utilize the glycolytic pathway to generate energy, whereas the DE cells formed from iPSCs use both glycolytic and oxidative phosphorylation pathways to generate energy, which is associated with a substantial increase in the initial OCR inside the cells. Hence, knowledge obtained through this study offers new insights into developing a robust stem cell differentiation procedure for generating human tissues.

### Author Contributions

**Sha Jin:** conceptualization, funding acquisition, project administration, supervision, formal analysis, methodology, writing – original draft, writing – review and editing. **Kaiming Ye:** conceptualization, funding acquisition, resources, writing – review and editing. **Hui Huang:** data curation, formal analysis, investigation, methodology, writing–original draft. The manuscript was written through the contributions of all authors. All authors have given approval to the final version of the manuscript.

### Acknowledgments

This work was partially supported by National Institutes of Health EB027391-01 and National Science Foundation CBET1928855 and CBET1919830.

### Conflicts of Interest

The authors declare no conflicts of interest.

### Data Availability Statement

The data that support the findings of this study are available upon reasonable request.

### References

1. C. Walsh and S. Jin, "Induced Pluripotent Stem Cells and CRISPR-Cas9 Innovations for Treating Alpha-1 Antitrypsin Deficiency and Glycogen Storage Diseases," *Cells* 13, no. 12 (2024): 1052.
2. D. A. Yefroyev and S. Jin, "Induced Pluripotent Stem Cells for Treatment of Alzheimer's and Parkinson's Diseases," *Biomedicines* 10, no. 2 (2022): 208.
3. E. S. Heaton and S. Jin, "Importance of Multiple Endocrine Cell Types in Islet Organoids for Type 1 Diabetes Treatment," *Translational Research* 250 (2022): 68–83.
4. D. A. Ogi and S. Jin, "Transcriptome-Powered Pluripotent Stem Cell Differentiation for Regenerative Medicine," *Cells* 12, no. 10 (2023): 1442.
5. A. Wesolowska-Andersen, R. R. Jensen, M. P. Alcantara, et al., "Analysis of Differentiation Protocols Defines a Common Pancreatic Progenitor Molecular Signature and Guides Refinement of Endocrine Differentiation," *Stem Cell Reports* 14 (2020): 138–153.

6. S. S. Karanth, S. Sun, H. Bi, K. Ye, and S. Jin, "Angiopoietins Stimulate Pancreatic Islet Development from Stem Cells," *Scientific Reports* 11 (2021): 13558.
7. H. Liu, R. Li, H. K. Liao, et al., "Chemical Combinations Potentiate Human Pluripotent Stem Cell-Derived 3D Pancreatic Progenitor Clusters Toward Functional  $\beta$  Cells," *Nature Communications* 12 (2021): 3330.
8. A. Rezaia, J. E. Bruin, P. Arora, et al., "Reversal of Diabetes With Insulin-Producing Cells Derived In Vitro From Human Pluripotent Stem Cells," *Nature Biotechnology* 32 (2014): 1121–1133.
9. Y. Jiang, C. Chen, L. N. Randolph, et al., "Generation of Pancreatic Progenitors From Human Pluripotent Stem Cells by Small Molecules," *Stem Cell Reports* 16 (2021): 2395–2409.
10. M. C. Nostro, F. Sarangi, C. Yang, et al., "Efficient Generation of NKX6-1+ Pancreatic Progenitors From Multiple Human Pluripotent Stem Cell Lines," *Stem Cell Reports* 4 (2015): 591–604.
11. M. Hu, T. Liu, H. Huang, et al., "Extracellular Matrix Proteins Refine Microenvironments for Pancreatic Organogenesis From Induced Pluripotent Stem Cell Differentiation," *Theranostics* 15 (2025): 2229–2249.
12. W. Wang, S. Jin, and K. Ye, "Development of Islet Organoids From H9 Human Embryonic Stem Cells in Biomimetic 3D Scaffolds," *Stem Cells and Development* 26 (2017): 394–404.
13. H. Huang, S. S. Karanth, Y. Guan, et al., "Oxygenated Scaffolds for Pancreatic Endocrine Differentiation From Induced Pluripotent Stem Cells," *Advanced Healthcare Materials* 13 (2024): 2302275.
14. G. G. Nair, J. S. Liu, H. A. Russ, et al., "Recapitulating Endocrine Cell Clustering in Culture Promotes Maturation of Human Stem-Cell-Derived  $\beta$  Cells," *Nature Cell Biology* 21 (2019): 263–274.
15. A. Super, N. Jaccard, M. P. C. Marques, et al., "Real-Time Monitoring of Specific Oxygen Uptake Rates of Embryonic Stem Cells in a Microfluidic Cell Culture Device," *Biotechnology Journal* 11 (2016): 1179–1189.
16. M. H. Kim, N. Thanuthanakhun, S. Fujimoto, and M. Kino-Oka, "Effect of Initial Seeding Density on Cell Behavior-Driven Epigenetic Memory and Preferential Lineage Differentiation of Human iPSCs," *Stem Cell Research* 56 (2021): 102534.
17. W. B. McIntyre, M. Karimzadeh, Y. Riazalhosseini, M. Khazaei, and M. G. Fehlings, "Cell-Cell Contact Mediates Gene Expression and Fate Choice of Human Neural Stem/Progenitor Cells," *Cells* 11, no. 11 (2022): 1741.
18. S. Jin, H. Yao, P. Krisanarungson, A. Haukas, and K. Ye, "Porous Membrane Substrates Offer Better Niches to Enhance the Wnt Signaling and Promote Human Embryonic Stem Cell Growth and Differentiation," *Tissue Engineering Part A* 18 (2012): 1419–1430.
19. T. Ezashi, P. Das, and R. M. Roberts, "Low O<sub>2</sub> Tensions and the Prevention of Differentiation of hES Cells," *Proceedings of the National Academy of Sciences of the United States of America* 102 (2005): 4783–4788.
20. F. Hakim, T. Kaitsuka, J. M. Raeed, et al., "High Oxygen Condition Facilitates the Differentiation of Mouse and Human Pluripotent Stem Cells into Pancreatic Progenitors and Insulin-Producing Cells," *Journal of Biological Chemistry* 289 (2014): 9623–9638.
21. K. A. D'Amour, A. D. Agulnick, S. Eliazar, O. G. Kelly, E. Kroon, and E. E. Baetge, "Efficient Differentiation of Human Embryonic Stem Cells to Definitive Endoderm," *Nature Biotechnology* 23 (2005): 1534–1541.
22. C. A. Fraker, S. Alvarez, P. Papadopoulos, et al., "Enhanced Oxygenation Promotes  $\beta$ -Cell Differentiation In Vitro," *Stem Cells* 25 (2007): 3155–3164.
23. E. Tsogtbaatar, C. Landin, K. Minter-Dykhouse, and C. D. L. Folmes, "Energy Metabolism Regulates Stem Cell Pluripotency," *Frontiers in Cell and Developmental Biology* 8 (2020): 87.
24. J. Zhang, E. Nuebel, G. Q. Daley, C. M. Koehler, and M. A. Teitell, "Metabolic Regulation in Pluripotent Stem Cells During Reprogramming and Self-Renewal," *Cell Stem Cell* 11 (2012): 589–595.
25. N. Shyh-Chang, Y. Zheng, J. W. Locasale, and L. C. Cantley, "Human Pluripotent Stem Cells Decouple Respiration From Energy Production," *EMBO Journal* 30 (2011): 4851–4852.
26. H. K. Wilson, S. G. Canfield, M. K. Hjortness, S. P. Palecek, and E. V. Shusta, "Exploring the Effects of Cell Seeding Density on the Differentiation of Human Pluripotent Stem Cells to Brain Microvascular Endothelial Cells," *Fluids Barriers CNS* 12 (2015): 13.
27. H. Zhou, M. D. Weir, and H. H. Xu, "Effect of Cell Seeding Density on Proliferation and Osteodifferentiation of Umbilical Cord Stem Cells on Calcium Phosphate Cement-Fiber Scaffold," *Tissue Engineering Part A* 17 (2011): 2603–2613.
28. H. Bi, K. Ye, and S. Jin, "Proteomic Analysis of Decellularized Pancreatic Matrix Identifies Collagen V as a Critical Regulator for Islet Organogenesis From Human Pluripotent Stem Cells," *Biomaterials* 233 (2020): 119673.
29. H. Bi, S. S. Karanth, K. Ye, R. Stein, and S. Jin, "Decellularized Tissue Matrix Enhances Self-Assembly of Islet Organoids From Pluripotent Stem Cell Differentiation," *ACS Biomaterials Science & Engineering* 6 (2020): 4155–4165.
30. E. L. Pearce and E. J. Pearce, "Metabolic Pathways in Immune Cell Activation and Quiescence," *Immunity* 38 (2013): 633–643.
31. C. D. Folmes, T. J. Nelson, A. Martinez-Fernandez, et al., "Somatic Oxidative Bioenergetics Transitions Into Pluripotency-Dependent Glycolysis to Facilitate Nuclear Reprogramming," *Cell Metabolism* 14 (2011): 264–271.
32. N. Hai, D. W. Shin, H. Bi, K. Ye, and S. Jin, "Mechanistic Analysis of Physicochemical Cues in Promoting Human Pluripotent Stem Cell Self-Renewal and Metabolism," *International Journal of Molecular Sciences* 19, no. 11 (2018): 3459.
33. N. J. Hogrebe, K. G. Maxwell, P. Augsornworawat, and J. R. Millman, "Generation of Insulin-Producing Pancreatic  $\beta$  Cells From Multiple Human Stem Cell Lines," *Nature Protocols* 16 (2021): 4109–4143.
34. M. P. Walczak, A. M. Drozd, E. Stoczynska-Fidelus, P. Rieske, and D. P. Grzela, "Directed Differentiation of Human iPSC Into Insulin Producing Cells Is Improved by Induced Expression of PDX1 and NKX6.1 Factors in IPC Progenitors," *Journal of Translational Medicine* 14 (2016): 341.
35. B. A. Wagner, S. Venkataraman, and G. R. Buettner, "The Rate of Oxygen Utilization by Cells," *Free Radical Biology and Medicine* 51 (2011): 700–712.
36. J. V. Chacko and K. W. Eliceiri, "Autofluorescence Lifetime Imaging of Cellular Metabolism: Sensitivity Toward Cell Density, pH, Intracellular, and Intercellular Heterogeneity," *Cytometry Part A* 95 (2019): 56–69.
37. W. Jones and K. Bianchi, "Aerobic Glycolysis: Beyond Proliferation," *Frontiers in Immunology* 6 (2015): 227.

## Supporting Information

Additional supporting information can be found online in the Supporting Information section.